

Volume Expansive Pressure (VEP) Driven Non-Trivial Topological Phase Transition In LiMgBi

Raghottam M Sattigeri^{1,a}, Sharad Babu Pillai^{1,b}, Prafulla K Jha^{1,c} and Brahmananda Chakraborty^{2,d}

¹*Department of Physics, Faculty of Science, The Maharaja Sayajirao University of Baroda, Vadodara.*

²*High Pressure and Synchrotron Radiation Physics Division, Bhabha Atomic Research Centre, Mumbai.*

Corresponding Authors: ^araghottam.ms@gmail.com, ^bsbpillai001@gmail.com, ^cprafullaj@yahoo.com, ^dbrahma@barc.gov.in

Abstract

Topological Insulators (TI) exhibit robust spin-locked dissipationless Fermion transport along the surface states. In the current study, we use *first-principles* calculations to investigate a Topological Phase Transition (TPT) in a Half-Heusler (HH) compound LiMgBi driven by a Volume Expansive Pressure (VEP) which is attributed to the presence of, intrinsic voids, thermal perturbations and/or due to a phenomena known as cavity nuclei. We find that, the dynamically stable *face-centred cubic* (FCC) structure of LiMgBi (which belongs to the $F\bar{4}3m[216]$ space group), undergoes TPT beyond a critical VEP (at 4.0%). The continuous application of VEP from 0.0% to 8.0% results in a phase transition from a, band insulator to a Dirac semi-metal nature. Qualitatively, the Dirac cone formation and band inversion along the high symmetry point Γ in the Brillouin Zone (BZ) are analysed in terms of Electronic Band Structure (EBS) and Projected Local Density of States (LDOS). The TPT is further characterised by the \mathbb{Z}_2 invariant, $(\nu_0, \nu_1 \nu_2 \nu_3) \equiv (1, 0 0 0)$ along the (0001) surface which indicates quantitatively that, HH LiMgBi is a *strong* TI. We hence propose, HH LiMgBi (known for its piezoelectric, thermo-electric and semi-conducting applications) as a strong TI with potential multi-purpose application in the field of electronics, spintronics and quantum computation.

Introduction

Topological Insulating (TI) phase of matter is interesting due to the exotic quantum properties such as, spin-locked dissipationless transport of Fermions along the topologically protected surfaces. As a result of this, the spin helicity along the surface has several potential applications in the field of spintronics, quantum computation etc.¹ Till date, several three dimensional (3D) materials have been predicted theoretically and some are realised experimentally²⁻⁶ to exhibit TI nature. A variety of 3D compounds (such as, Bi_2Se_3 , $\beta\text{-As}_2\text{Te}_3$, AMgBi ($A = \text{Li, Na, K}$) and elemental tellurium (Te)) exhibit TI nature driven by strain.⁷⁻⁹ These materials also have multi-purpose applications.¹⁰⁻¹² It is known that, specific electronic properties of material depend explicitly on their crystal structure and associated space group. This implies that, crystals of different structural class with previously known applications can be designed precisely to investigate for the Topological Phase Transition (TPT) by employing well known band engineering technique which is based on application of strain or pressure (compressive or expansive in nature).

Strain engineering of the electronic band structure is utilized to realize a strong TI.^{7,8} This is because, the application of strain / pressure enhances the strength of Spin Orbit Coupling (SOC) in some systems.⁸ But,

there are systems such as, 3D elemental Te (three fold screw symmetric helical chains of Te atoms) where, it is observed that, weak van der Waals interaction between the helical layered arrangement of Te atoms can be manipulated by application of shear strain (violates three fold screw symmetry of helices) and hydrostatic pressure leading to band inversion which is a characteristic property of a TI system.⁹ This suggests that, without venturing into the computationally costly; SOC calculations, simple application of strain or pressure can yield the desired TPT in materials.^{9,13} One such system is, Anti-Ferroelectric TI (AFTI) material AMgBi (A = Li, Na, K) which exhibits strong TI nature characterized by the \mathbb{Z}_2 invariant $\nu = 1$ in both Pnma and P6₃mc structures.¹³ This is achieved under the influence of epitaxial strain and hydrostatic pressure.¹³ Of these, the most promising candidate TI was found to be LiMgBi under epitaxial strain leading to AFTI of Type I (represents normal anti-polar and topological polar states).¹³

LiMgBi which belongs to Pnma and P6₃mc space groups and exhibits AFTI of Type I¹³ also exists as a Half Heusler (HH) compound (in the form PQR where, P and Q are transition metals and R is a p-block element) with a variety of applications such as a semi-conducting, piezoelectric and thermo-electric material.^{11,12,14} Theoretical search for TI nature in HH compounds has been pursued since a long time.¹⁵ Concrete efforts have led to theoretical predictions of HH compounds as candidate TIs.¹⁶⁻²⁴ Also, there are studies where, strain tuning led to realization of TI nature in materials.²³⁻²⁷ We perform analogous calculations to investigate TPT in *Face-Centred Cubic* (FCC) HH LiMgBi described by the F $\bar{4}$ 3m[216] space group in Hermann-Mauguin representation. Experimentally it is observed that, LiMgBi in FCC phase exhibits *trivial* band insulating behaviour.¹¹ One study suggests that, when screening potential method is employed,²⁸ a large number of candidate HH compounds can be classified as TI and Normal Insulator (NI). Based on this study it turns out that, thirty three HH compounds exhibit TI nature, but, LiMgBi exhibits NI nature at ambient conditions. Feng et.al. show that, strain tuning of band order in cubic systems can lead to TI nature.²⁵

With this background, we investigate the possibility of TPT in FCC LiMgBi by strain tuning the band order which is quite uncharted. We find that, under Volume Expansive Pressure (VEP), HH LiMgBi undergoes a TPT at a critical value of 4.0% and exhibits a strong TI nature characterized by the \mathbb{Z}_2 invariant as (1, 0 0 0). Thus, indicating that, HH LiMgBi is a candidate TI material for novel applications in the field of spintronics, quantum computation etc.

Methodology

We performed density functional theory based *first-principles* calculations to investigate TPT under the application of pressure. For this purpose, we obtained crystallographic information for LiMgBi in F $\bar{4}$ 3m[216] space group from MaterialsProject repository.²⁹ Optimization of lattice constant (a) was performed following the convergence test for total energy with respect to, wave function cut off and **k**-mesh. We used norm conserving pseudopotentials under Generalized Gradient Approximation (GGA) which considers 1s¹, 3s² and 6s²6p³ orbitals of Li, Mg and Bi respectively. The pseudopotential method is based on Martins-Troullier with exchange correlation of Perdew-Burke-Ernzerhof (PBE) functional type.³⁰ The optimization was performed by, finding a

global minima in terms of the total energy of the system and then narrowing down (using bisection method) to a local minima with a constrain that, the total pressure on the atoms is 0.00 kbar. The converged value of plane wave kinetic energy cut-off and charge density are 50 Ry and 200 Ry respectively. A uniform Monkhorst-Pack Grid³¹ for \mathbf{k} -points of $7 \times 7 \times 7$ was used in the self-consistent calculations. For better prediction of energy band gap,³² we performed calculations with Heyd–Scuseria–Ernzerhof (HSE06) screened Coulomb hybrid functional³³ in Vienna *ab initio* simulation package (VASP)³⁴ with proper optimization. Phonon calculations were performed using Density Functional Perturbation Theory (DFPT).³⁵ For phonon calculations, we used $10 \times 10 \times 10$ \mathbf{q} -mesh which was followed by plotting the dynamical matrices in the entire Brillouin Zone (BZ). Following the analysis of structural and dynamic stability, we performed electronic calculations pertaining to the Electronic Band Structure (EBS), Density of States (DOS) and Surface States (SS). Optimization and electronic properties were calculated using the QUANTUM ESPRESSO code³⁶ while the SS were calculated using WannierTools (WT)³⁷ package which employed the Wannier Function Centres (WFC) obtained from a post processing package Wannier90 (W90).³⁸ The electronic properties led to qualitative results whereas for quantitative characterization of the TI nature, WT package was used for thorough \mathbb{Z}_2 analysis.

Results and Discussion

Structural Properties and Dynamic Stability

The optimized value of the lattice constant (a) under GGA approximation is 6.81 Å. This value is in descent agreement with the experimental (6.74 Å) and other theoretical (6.71 Å) values.¹¹ The optimized crystal structure is shown in Figure 1 which was found to be dynamically stable. The primitive cell vectors for HH LiMgBi are defined in terms of lattice constant ‘ a ’ as, $\mathbf{v}_1 = (a/2)(-1,0,1)$, $\mathbf{v}_2 = (a/2)(0,1,1)$, $\mathbf{v}_3 = (a/2)(-1,1,0)$ with atoms Li, Mg and Bi occupying, $4b$, $4c$ and $4a$ Wyckoff positions respectively.³⁹ This structure results in a direct Band Gap (BG) as seen from the EBS presented in Figure 2 which is quite small as compared to previous studies (Table 1). Since it is known that, the error in BG prediction is smaller in HSE calculations as compared to pure DFT calculations,³² we performed HSE calculations at 0.0%, 4.0% and 6.5% VEP. The BG from HSE calculations are in strong agreement (Table 1) with previous studies and better than the GGA calculations.

	Work	LiMgBi
Lattice Constant (Å)	PBE	6.81
	Theory ¹¹	6.71
	Experiment ^{11, 40}	6.74
Energy Band Gap (eV)	PBE	0.35
	PBE+HSE	0.70
	Theory ¹¹	0.62
	Experiment	-

Table 1: Theoretical and experimental values of lattice constant (a) and energy band gap.

We increase lattice constant (a) in steps of 0.5% from 0.0% to 8.0% to investigate for TPT in HH LiMgBi. We refer to this increment as VEP which can be attributed to an effect created by the presence of an intrinsic

void (exerting a volume isotropic pressure in the outward direction) in the crystal structure or due to extreme internal *thermal* perturbations. Also, it can be attributed to experimentally observed phenomena such as *cavitation* pressure⁴¹ due to impurities known as *cavity nuclei*. Increment in unit cell volume (a.u.³) due to application of VEP (Figure 3) is interpreted in terms of volume strain as shown in Figure 4. Also, we analyse the difference in Total Energy ($\Delta E = E_i - E_0$) of the system (in Ry units) with respect to % VEP (Figure 5) due to the volume strain and find that, due to increment in VEP, the system deviates from its equilibrium state leading to a quantum phase transition.

Phonon dispersion calculations were performed to check the lattice dynamical stability of the proposed crystal system LiMgBi belonging to the $F\bar{4}3m[216]$ space group. This is important because, Phonon studies are fundamental in underpinning the vibrational dynamics in a phase transition and the practical feasibility to synthesize the material.⁴² In the current study, Phonon Dispersion Curves (PDC) are obtained as shown in Figure 6 at 0% VEP. As there are three (3) atoms in the unit cell of LiMgBi, we obtain nine (9) Phonon branches in the dispersion relation (Figure 6). The PDC shows that, the system LiMgBi is, dynamically stable and has no imaginary modes of vibration. From Figure 6, we can see that, in the lower frequency regime there are 3 modes which correspond to the acoustic branches and in the higher frequency regime, there are six ($3N - 3$, here $N = 3$) optical modes.⁴³ The acoustic branch exhibits one (in plane) Longitudinal Acoustic (LA) and two (in plane) Transverse Acoustic (TA) modes of vibration which are degenerate along the directions, \mathbf{W} to \mathbf{X} and \mathbf{L} to $\mathbf{\Gamma}$ in the BZ. The optical branch exhibits two ($N - 1$, here $N = 3$) Longitudinal Optical (LO) and four ($2N - 2$, here $N = 3$) Transverse Optical modes of vibration which dominate in the higher frequency regime.⁴³ The TO modes are degenerate along the directions $\mathbf{\Gamma}$ to \mathbf{K} , \mathbf{K} to \mathbf{X} and \mathbf{X} to $\mathbf{\Gamma}$ in the BZ. Similarly, the LO modes are degenerate at $\mathbf{\Gamma}$ in the BZ.

With proper understanding of the structural and dynamic stability of LiMgBi, we proceed for further analysis. We shall broadly divide our discussions here off in two perspectives, *qualitative* which revolves around the electronic properties and *quantitative* which revolves around the \mathbb{Z}_2 analysis.

Electronic Properties and Surface States

EBS analysis has proved to be a fruitful *qualitative* method to look for TI nature in materials.^{6-9,13,44,45} We hence, analyse the EBS for band inversion by band engineering which is a characteristic signatures of TI nature. It is observed that, band inversion occurs in LiMgBi when subjected to VEP in steps of 0.5% at a critical value of 4.0%. From the EBS we observe a phase transition from a band insulator like behaviour to a Dirac semi-metal like behaviour. A direct BG (0.35 eV and 0.70 eV from PBE and HSE06 calculations respectively) exists at high symmetry point ($\mathbf{\Gamma}$) in the BZ at 0% VEP (Figure 7). This is compared to previous studies (Table 1) where the band gap is ~ 0.62 eV.¹¹ BG from our HSE calculations match closely with the BG from previous studies.¹¹ For qualitative analysis we continue to discuss the electronic properties in terms of band gap under GGA and HSE approximation (tabulated in Table 2 for three different values of % VEP).

It is observed from the band structure that, the Valence Band (VB) maxima has a doubly degenerate state along the high symmetry point $\mathbf{\Gamma}$ whereas, the Conduction Band (CB) minima has single non-degenerate state

Functional	% VEP	Band Gap (eV)
	0.0	0.35
GGA	4.0	0.00
	6.5	0.001
	0.0	0.70
HSE	4.0	0.00
	6.5	0.10

Table 2: Energy band gap from GGA and HSE calculations at 0.0%, 4.0% (critical VEP) and 6.5% VEP.

along the high symmetry point Γ . This feature is protected by the two-fold symmetry of the FCC structure. With the gradual increment of VEP, at 4.0% VEP, LiMgBi undergoes a phase transition from band insulator nature to a Dirac semi-metal nature (Figure 7) with BG 0.00 eV. We represent the eigen states along the high symmetry line Γ as Γ_i where ‘ i ’ is the band index without inclusion of spin degeneracy. The EBS for 0%, 4.0% and 6.5% are shown in Figure 7. At 0% VEP the band order is Γ_6 (dominated by p orbital), Γ_8 (dominated by p orbital) and Γ_{10} (dominated by s orbital). Here, Γ_6 and Γ_8 bands are degenerate as seen in Figure 7(a). With increment in VEP, at 4.0% a Dirac Cone is formed as shown in Figure 7(b). This feature exhibits a linear dissipationless transport of Fermions along the surface of LiMgBi. Also, the formation of a Dirac Cone leads to degeneracy between Γ_8 and Γ_{10} bands as seen in Figure 7(b). The formation of Dirac cone also, lifts up the degeneracy between bands Γ_6 and Γ_8 . By further increment in VEP, BG reopens with to 1.1 meV (under GGA) as shown in Figure 7(c) and 0.10 eV (under HSE). This reopening characterizes the band inversion in terms of the inversion in band order with, Γ_8 (dominated by p orbital) being exchanged with Γ_{10} (dominated by s orbital) wherein, Γ_{10} feature is transferred to Γ_6 (dominated by p orbital) band. Also, as the CB crosses Fermi level it indicates that, LiMgBi exhibits conduction of Fermions along the surface.

In order to justify the band inversion, we discuss the orbital contributions of Li, Mg and Bi. For this purpose, projected LDOS were calculated to compliment the EBS. We refrain our discussions to the regions in the vicinity of Fermi energy level (E_F) which is important for interpretation of band inversion. At 0% VEP, the LDOS is as shown in Figure 8. VB in the vicinity of Fermi level in Li is dominated by a small contribution from unhybridized ‘ s ’ orbital, while the CB is dominated majorly by unhybridized ‘ s ’ orbital. Similarly, the VB in Mg has small contributions from the ‘ s ’ orbitals and the CB has major contribution from the ‘ s ’ orbital, both being unhybridized. In both the cases (Li and Mg), the ‘ s ’ orbital contribution from the CB crosses Fermi energy level (E_F) as seen from Figure 8. As compared to this, Bi has a strong contribution solely due to the ‘ p ’ orbital in VB with a strong hybridization with the ‘ s ’ orbital in CB. Also, in the VB a mild contribution from the ‘ s ’ orbital is observed but, near Fermi energy level (E_F) the ‘ s ’ orbital has major contribution as seen in Figure 8. Beyond a critical value of VEP at 4.5% the orbital contributions for the Dirac cone formation at the Dirac point on the Fermi energy level (E_F) are interpreted from the LDOS as shown in Figure 9. The VB and CB of Li and Mg are dominated by the ‘ s ’ orbital with a increment in its orbital contribution at E_F indicating the formation of Dirac cone (Figure 9). Although, the CB in both (Li and Mg) retains the ‘ s ’ orbital dominant feature. Similarly, in Bi, the major contribution for Dirac cone formation comes from the VB ‘ p ’ orbital crossing the Fermi energy level (E_F) which has a weak hybridization with ‘ s ’ orbital, the strong hybridization persists and dominates the

deeper regions of CB (Figure 9). At 6.5% of VEP when the band reopens, the orbital contributions change as compared to the 0% and 4.5% case above. Figure 10 shows the LDOS at 6.5% VEP. From the LDOS for Li and Mg, we observe that, the orbital contribution due to ‘s’ orbital increases in the VB region (Figure 10). Similarly from the LDOS for Bi, the ‘p’ orbital contribution reduces in the VB and increases in the interior regions of CB with a strong hybridization with the ‘s’ orbitals, whereas, the ‘s’ orbital contribution is almost negligible in VB but increases slightly in the interior of VB. The changes observed in the orbital contributions are contemplated as an indicator of the band order rearrangement observed in the EBS, which is a characteristic signature of band inversion. The major contribution for the band inversion is due to the Bi which has strong share in orbital rearrangements.

Further analysis for a deeper realization of TI behaviour was performed by calculating the SS. Figure 11 is the computational Angle Resolved Photo Emission Spectra (ARPES)^{6,46,47} showing the SS⁴⁸ at 0% and 4.5% VEP respectively. Beyond the critical value of VEP (i.e., beyond 4.0% VEP) we observe dissipationless Fermi Surface along the edge states in the BZ. This is a qualitative evidence of TI nature characterized by, a *single* Dirac cone SS (similar to previous work⁴⁹). This predicts that, experimental realization of FCC LiMgBi can be characterized by performing ARPES to examine the SS along the (0001) surface.

\mathbb{Z}_2 Analysis

The \mathbb{Z}_2 invariant is essential to characterize a material into a \mathbb{Z}_2 topological class. There are various methods to obtain the \mathbb{Z}_2 invariant^{2,50–53} for systems with and without inversion symmetry. Generally, for systems with inversion symmetry, the product of parities of eigen values is calculated at eight (8) Time Reversal Invariant Momenta (TRIM) points for a 3D system (equation 1) and at four (4) TRIM points for a two dimensional (2D) system.² The \mathbb{Z}_2 invariant $\nu_0 = 1$ and $\nu_0 = 0$ corresponds to strong and weak TI respectively.^{2,6} Evolution of \mathbb{Z}_2 invariant along the application of pressure is shown in Figure 12. Since, the system is FCC, which lacks inversion symmetry, the \mathbb{Z}_2 analysis was performed by calculating the \mathbb{Z}_2 invariants $(\mathbb{Z}_2)_\pi$ and $(\mathbb{Z}_2)_0$, for two different planes of momentum (k) in the BZ resulting in the \mathbb{Z}_2 invariant ν_0 as, $\nu_0 = [(\mathbb{Z}_2)_\pi - (\mathbb{Z}_2)_0] \pmod{2}$. These calculations were performed using the WannierTools (WT) package³⁷ which utilizes the information regarding the Wannier Function Centres (WFC) obtained by post processing package Wannier90 (W90).³⁸ Maximally Localised Wannier Functions (MLWF) were obtained after PWSCF calculations using Marzari and Vanderbilt (MV) method in W90 package. The MV method minimizes the gauge dependent spread $\tilde{\Omega}$ with respect to the Bloch states $U^{(k)}$ which are obtained from the PWSCF calculations.³⁶ The WFC are then used for computation of Wilson Loops in WT. WT was used to obtain Tight Binding (TB) model for LiMgBi using the MLWF from W90. Using this TB model, we compute the \mathbb{Z}_2 invariant by calculating the Wilson loops around the Wannier Charge Centres (WCC). This method is one of the best methods for systems without inversion symmetry.³⁷ Computational APRES is obtained using WT along the (0001) crystal direction. WT is a reliable software used quite often for such studies.^{51,54–57}

$$(-1)^{\nu_i} = \prod_{i=1}^8 \delta(\Lambda_i) \quad (1)$$

$$\nu_0 = \left(\mathbb{Z}_2(k_i = 0) + \mathbb{Z}_2(k_i = 0.5) \right) \text{mod} 2 \quad (2)$$

$$\nu_i = \mathbb{Z}_2(k_i = 0.5) \quad (3)$$

The underlying computation in WT is carried out along the six Time Reversal Invariant Planes (TRIP) $k_x = 0, \pi$, $k_y = 0, \pi$ and $k_z = 0, \pi$ in the BZ. The \mathbb{Z}_2 indices $(\nu_0, \nu_1, \nu_2, \nu_3)$ are computed using equation 2 and 3.³⁷ Based on these calculations, LiMgBi under 0% VEP is characterized by \mathbb{Z}_2 invariant $\nu_0 = 0$ which implies that LiMgBi is a weak TI. But, beyond the critical value of VEP, at 4.5% the \mathbb{Z}_2 indices are obtained to be $(\nu_0, \nu_1, \nu_2, \nu_3) \equiv (1, 0, 0, 0)$ which implies that, LiMgBi is a strong TI. Thus we conclude quantitatively that, LiMgBi undergoes a TPT under the application of VEP.

Conclusion

In summary, we performed density functional theory based *first-principles* calculations and find that, HH compound LiMgBi which was previously studied for its semi-conducting, piezoelectric and thermo-electric properties undergoes a TPT driven by VEP. The FCC structure of LiMgBi was subjected to VEP isotropically by increment of the lattice constant (a). At equilibrium, the EBS has a direct BG of ~ 0.35 eV (under GGA) and ~ 0.70 eV (under HSE06). With gradual increment in VEP, we find a critical value at which, LiMgBi undergoes a *phase transition* from a trivial band insulator to a Dirac semi-metal material. With further increment in VEP, the band reopening is observed which is quite small; with a BG of the order of ~ 1.1 meV (under GGA) and ~ 0.10 eV (under HSE) indicating, band inversion due to exchange of orbital contribution in the VBM and CBM. This was complemented by thorough analysis of projected LDOS in order to understand the orbital contribution of the constituent elements. In order to indicate experimental characterization of the TI nature, SS were calculated using computational ARPES along the direction (0001) which exhibits the presence of a surface Dirac cone. These results were further quantified by studying the evolution of \mathbb{Z}_2 invariant along the application VEP. The strong TI nature of HH LiMgBi is characterized by the \mathbb{Z}_2 index, $(\nu_0, \nu_1, \nu_2, \nu_3) \equiv (1, 0, 0, 0)$. We thus conclude that, HH compound LiMgBi with FCC crystal structure undergoes a TPT driven by VEP. These calculations will open up diverse perspectives for multi-purpose applications of LiMgBi as a strong TI apart from the known semi-conducting, piezoelectric and thermo-electric applications.

Acknowledgement

Authors acknowledge, Department of Science and Technology (DST), Government of India, for providing financial assistance.

References

- [1] Joel E Moore. The birth of topological insulators. *Nature*, 464(7286):194, 2010.
- [2] Liang Fu, Charles L Kane, and Eugene J Mele. Topological insulators in three dimensions. *Physical review letters*, 98(10):106803, 2007.
- [3] M Zahid Hasan and Charles L Kane. Colloquium: topological insulators. *Reviews of modern physics*, 82(4):3045, 2010.
- [4] M Zahid Hasan and Joel E Moore. Three-dimensional topological insulators. *Annu. Rev. Condens. Matter Phys.*, 2(1):55–78, 2011.
- [5] Xiao-Liang Qi and Shou-Cheng Zhang. Topological insulators and superconductors. *Reviews of Modern Physics*, 83(4):1057, 2011.
- [6] Yoichi Ando. Topological insulator materials. *Journal of the Physical Society of Japan*, 82(10):102001, 2013.
- [7] H Aramberri and MC Muñoz. Strain-driven tunable topological states in Bi_2Se_3 . *Journal of Physics: Materials*, 1(1):015009, 2018.
- [8] Koushik Pal and Umesh V Waghmare. Strain induced z^2 topological insulating state of $\beta\text{-As}_2\text{Te}_3$. *Applied Physics Letters*, 105(6):062105, 2014.
- [9] Luis A Agapito, Nicholas Kioussis, William A Goddard III, and Nai Phuan Ong. Novel family of chiral-based topological insulators: elemental tellurium under strain. *Physical review letters*, 110(17):176401, 2013.
- [10] F Casper, T Graf, S Chadov, B Balke, and C Felser. Half-Heusler compounds: novel materials for energy and spintronic applications. *Semiconductor Science and Technology*, 27(6):063001, 2012.
- [11] Anindya Roy, Joseph W Bennett, Karin M Rabe, and David Vanderbilt. Half-Heusler semiconductors as piezoelectrics. *Physical review letters*, 109(3):037602, 2012.
- [12] Manoj K Yadav and Biplab Sanyal. First principles study of thermoelectric properties of Li-based half-Heusler alloys. *Journal of Alloys and Compounds*, 622:388–393, 2015.
- [13] Bartomeu Monserrat, Joseph W Bennett, Karin M Rabe, and David Vanderbilt. Antiferroelectric topological insulators in orthorhombic AMgBi compounds ($A = \text{Li, Na, K}$). *Physical review letters*, 119(3):036802, 2017.
- [14] E Mooser. Semiconducting compounds. *Science*, 132(3436):1285–1291, 1960.
- [15] Shi-Yuan Lin, Ming Chen, Xiao-Bao Yang, Yu-Jun Zhao, Shu-Chun Wu, Claudia Felser, and Binghai Yan. Theoretical search for half-Heusler topological insulators. *Physical Review B*, 91(9):094107, 2015.

- [16] Di Xiao, Yugui Yao, Wanxiang Feng, Jun Wen, Wenguang Zhu, Xing-Qiu Chen, G Malcolm Stocks, and Zhenyu Zhang. Half-Heusler compounds as a new class of three-dimensional topological insulators. *Physical Review Letters*, 105(9):096404, 2010.
- [17] Hsin Lin, L Andrew Wray, Yuqi Xia, Suyang Xu, Shuang Jia, Robert J Cava, Arun Bansil, and M Zahid Hasan. Half-Heusler ternary compounds as new multifunctional experimental platforms for topological quantum phenomena. *Nature materials*, 9(7):546, 2010.
- [18] Binghai Yan and Anne de Visser. Half-Heusler topological insulators. *MRS Bulletin*, 39(10):859–866, 2014.
- [19] Chang Liu, Yongbin Lee, Takeshi Kondo, Eun Deok Mun, Malinda Caudle, Bruce N Harmon, Sergey L Bud'ko, Paul C Canfield, and Adam Kaminski. Metallic surface electronic state in half-Heusler compounds r PtBi ($r = \text{Lu, Dy, Gd}$). *Physical Review B*, 83(20):205133, 2011.
- [20] XT Wang, XF Dai, HY Jia, LY Wang, XF Liu, YT Cui, and GD Liu. Topological insulating characteristic in half-Heusler compounds composed of light elements. *Physics Letters A*, 378(22-23):1662–1666, 2014.
- [21] C Li and Z Wen. Electronic structure of topological insulators with mm' x half-Heusler compounds using density functional theory. *Thin Solid Films*, 546:436–438, 2013.
- [22] Kulwinder Kaur and Ranjan Kumar. Ti based half Heusler compounds: A new one on the screen with robust thermoelectric performance. *Journal of Alloys and Compounds*, 727:1171–1177, 2017.
- [23] Joel Moore. Topological insulators: The next generation. *Nature Physics*, 5(6):378, 2009.
- [24] Marcel Franz. Topological insulators: Starting a new family. *Nature materials*, 9(7):536, 2010.
- [25] Wanxiang Feng, Wenguang Zhu, Hanno H Weitering, G Malcolm Stocks, Yugui Yao, and Di Xiao. Strain tuning of topological band order in cubic semiconductors. *Physical Review B*, 85(19):195114, 2012.
- [26] Wanxiang Feng, Di Xiao, Jun Ding, and Yugui Yao. Three-dimensional topological insulators in $i\text{-iii-vi}_2$ and ii-iv-v_2 chalcopyrite semiconductors. *Physical Review Letters*, 106(1):016402, 2011.
- [27] Junwei Liu, Yong Xu, Jian Wu, Bing-Lin Gu, SB Zhang, and Wenhui Duan. Manipulating topological phase transition by strain. *Acta Crystallographica Section C: Structural Chemistry*, 70(2):118–122, 2014.
- [28] Jianghui Liu, Huijun Liu, Guohua Cao, and Zizhen Zhou. Screening for potential topological insulators in half-Heusler compounds via compressed-sensing. *arXiv preprint arXiv:1808.04748*, 2018.
- [29] Anubhav Jain, Shyue Ping Ong, Geoffroy Hautier, Wei Chen, William Davidson Richards, Stephen Dacek, Shreyas Cholia, Dan Gunter, David Skinner, Gerbrand Ceder, and Kristin a. Persson. The Materials Project: A materials genome approach to accelerating materials innovation. *APL Materials*, 1(1):011002, 2013.
- [30] JP Perdew, K Burke, and M Ernzerhof. Perdew, burke, and ernzerhof reply. *Physical Review Letters*, 80(4):891, 1998.

- [31] Hendrik J Monkhorst and James D Pack. Special points for brillouin-zone integrations. *Physical review B*, 13(12):5188, 1976.
- [32] Jochen Heyd and Gustavo E Scuseria. Efficient hybrid density functional calculations in solids: Assessment of the heyd–scuseria–ernzerhof screened coulomb hybrid functional. *The Journal of chemical physics*, 121(3):1187–1192, 2004.
- [33] Jochen Heyd, Gustavo E Scuseria, and Matthias Ernzerhof. Hybrid functionals based on a screened coulomb potential. *The Journal of chemical physics*, 118(18):8207–8215, 2003.
- [34] G. Kresse and J. Furthmüller. Efficient iterative schemes for ab initio total-energy calculations using a plane-wave basis set. *Phys. Rev. B*, 54:11169–11186, Oct 1996.
- [35] Stefano Baroni, Stefano de Gironcoli, Andrea Dal Corso, and Paolo Giannozzi. Phonons and related crystal properties from density-functional perturbation theory. *Rev. Mod. Phys.*, 73:515–562, Jul 2001.
- [36] P Giannozzi, O Andreussi, T Brumme, O Bunau, M Buongiorno Nardelli, M Calandra, R Car, C Cavazzoni, D Ceresoli, M Cococcioni, N Colonna, I Carnimeo, A Dal Corso, S de Gironcoli, P Delugas, R A DiStasio Jr, A Ferretti, A Floris, G Fratesi, G Fugallo, R Gebauer, U Gerstmann, F Giustino, T Gorni, J Jia, M Kawamura, H-Y Ko, A Kokalj, E Küçükbenli, M Lazzeri, M Marsili, N Marzari, F Mauri, N L Nguyen, H-V Nguyen, A Otero de-la Roza, L Paulatto, S Poncé, D Rocca, R Sabatini, B Santra, M Schlipf, A P Seitsonen, A Smogunov, I Timrov, T Thonhauser, P Umari, N Vast, X Wu, and S Baroni. Advanced capabilities for materials modelling with quantum espresso. *Journal of Physics: Condensed Matter*, 29(46):465901, 2017.
- [37] Wanniertools : An open-source software package for novel topological materials. *Computer Physics Communications*, 224:405 – 416, 2018.
- [38] An updated version of wannier90: A tool for obtaining maximally-localised wannier functions. *Computer Physics Communications*, 185(8):2309 – 2310, 2014.
- [39] Wael Al-Sawai, Hsin Lin, RS Markiewicz, LA Wray, Y Xia, S-Y Xu, MZ Hasan, and A Bansil. Topological electronic structure in half-heusler topological insulators. *Physical Review B*, 82(12):125208, 2010.
- [40] Alec Belsky, Mariette Hellenbrandt, Vicky Lynn Karen, and Peter Luksch. New developments in the inorganic crystal structure database (icsd): accessibility in support of materials research and design. *Acta Crystallographica Section B: Structural Science*, 58(3):364–369, 2002.
- [41] Eric Herbert, Sébastien Balibar, and Frédéric Caupin. Cavitation pressure in water. *Physical Review E*, 74(4):041603, 2006.
- [42] Sharad Babu Pillai, Shweta D Dabhi, Som Narayan, and Prafulla K Jha. Strain effect on electronic and lattice dynamical behaviour of two dimensional bi, bias and bisb. In *AIP Conference Proceedings*, volume 1942, page 090022. AIP Publishing, 2018.

- [43] Gang Chen. *Nanoscale energy transport and conversion: a parallel treatment of electrons, molecules, phonons, and photons*. Oxford University Press, 2005.
- [44] Stanislav Chadov, Xiaoliang Qi, Jürgen Kübler, Gerhard H Fecher, Claudia Felser, and Shou Cheng Zhang. Tunable multifunctional topological insulators in ternary heusler compounds. *Nature materials*, 9(7):541, 2010.
- [45] Jinsong Zhang, Cui-Zu Chang, Zuocheng Zhang, Jing Wen, Xiao Feng, Kang Li, Minhao Liu, Ke He, Lili Wang, Xi Chen, et al. Band structure engineering in (bi 1- x sb x) 2 te 3 ternary topological insulators. *Nature communications*, 2:574, 2011.
- [46] YL Chen, James G Analytis, J-H Chu, ZK Liu, S-K Mo, Xiao-Liang Qi, HJ Zhang, DH Lu, Xi Dai, Zhong Fang, et al. Experimental realization of a three-dimensional topological insulator, bi2te3. *science*, 325(5937):178–181, 2009.
- [47] David Hsieh, Yuqi Xia, D Qian, L Wray, Fabian Meier, JH Dil, J Osterwalder, L Patthey, AV Fedorov, H Lin, et al. Observation of time-reversal-protected single-dirac-cone topological-insulator states in bi 2 te 3 and sb 2 te 3. *Physical review letters*, 103(14):146401, 2009.
- [48] Xiangang Wan, Ari M. Turner, Ashvin Vishwanath, and Sergey Y. Savrasov. Topological semimetal and fermi-arc surface states in the electronic structure of pyrochlore iridates. *Phys. Rev. B*, 83:205101, May 2011.
- [49] Yuqi Xia, Dong Qian, David Hsieh, L Wray, Arijeet Pal, Hsin Lin, Arun Bansil, DHYS Grauer, Yew San Hor, Robert Joseph Cava, et al. Observation of a large-gap topological-insulator class with a single dirac cone on the surface. *Nature physics*, 5(6):398, 2009.
- [50] Dominik Gresch, Gabriel Autes, Oleg V Yazyev, Matthias Troyer, David Vanderbilt, B Andrei Bernevig, and Alexey A Soluyanov. Z2pack: Numerical implementation of hybrid wannier centers for identifying topological materials. *Physical Review B*, 95(7):075146, 2017.
- [51] Alexey A Soluyanov and David Vanderbilt. Computing topological invariants without inversion symmetry. *Physical Review B*, 83(23):235401, 2011.
- [52] Takahiro Fukui and Yasuhiro Hatsugai. Quantum spin hall effect in three dimensional materials: Lattice computation of z2 topological invariants and its application to bi and sb. *Journal of the Physical Society of Japan*, 76(5):053702, 2007.
- [53] Rui Yu, Xiao Liang Qi, Andrei Bernevig, Zhong Fang, and Xi Dai. Equivalent expression of z 2 topological invariant for band insulators using the non-abelian berry connection. *Physical Review B*, 84(7):075119, 2011.
- [54] Rui Yu, Hongming Weng, Zhong Fang, Xi Dai, and Xiao Hu. Topological node-line semimetal and dirac semimetal state in antiperovskite cu 3 pdn. *Physical review letters*, 115(3):036807, 2015.

- [55] Hongming Weng, Yunye Liang, Qiunan Xu, Rui Yu, Zhong Fang, Xi Dai, and Yoshiyuki Kawazoe. Topological node-line semimetal in three-dimensional graphene networks. *Physical Review B*, 92(4):045108, 2015.
- [56] Ronghan Li, Hui Ma, Xiyue Cheng, Shoulong Wang, Dianzhong Li, Zhengyu Zhang, Yiyi Li, and Xing-Qiu Chen. Dirac node lines in pure alkali earth metals. *Physical review letters*, 117(9):096401, 2016.
- [57] Tomáš Bzdušek, QuanSheng Wu, Andreas Rüegg, Manfred Sigrist, and Alexey A Soluyanov. Nodal-chain metals. *Nature*, 538(7623):75, 2016.

Figures

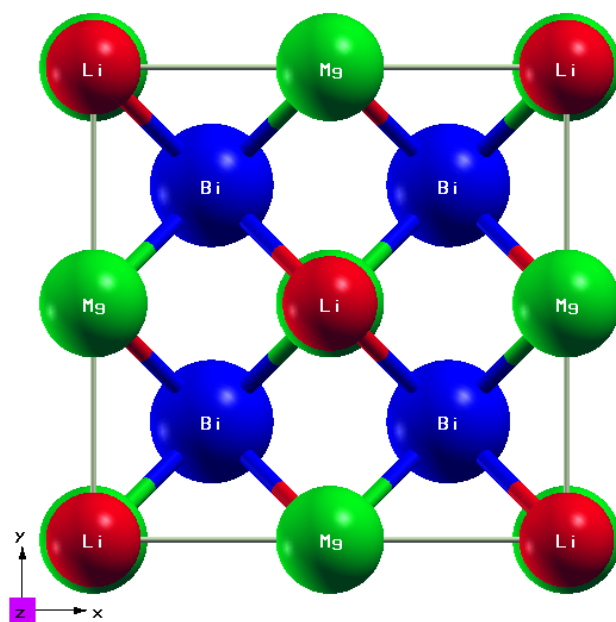


Figure 1: FCC structure of LiMgBi with lattice constant (a) $\sim 6.81 \text{ \AA}$

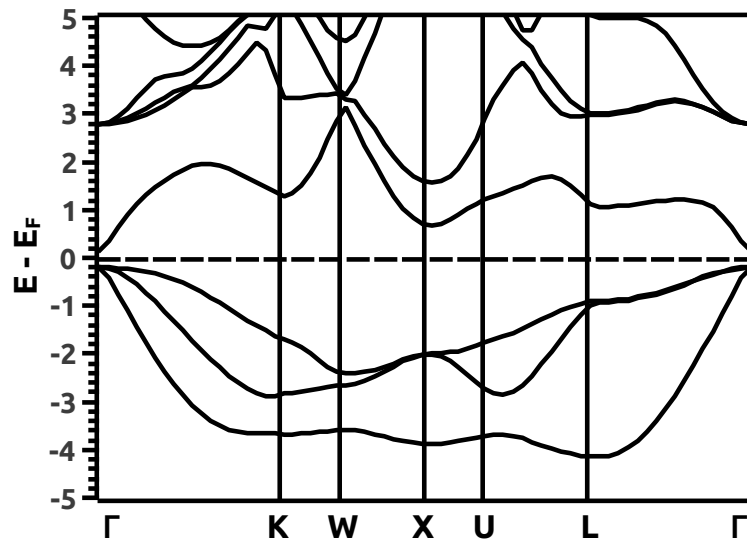


Figure 2: Electronic band structure of HH LiMgBi

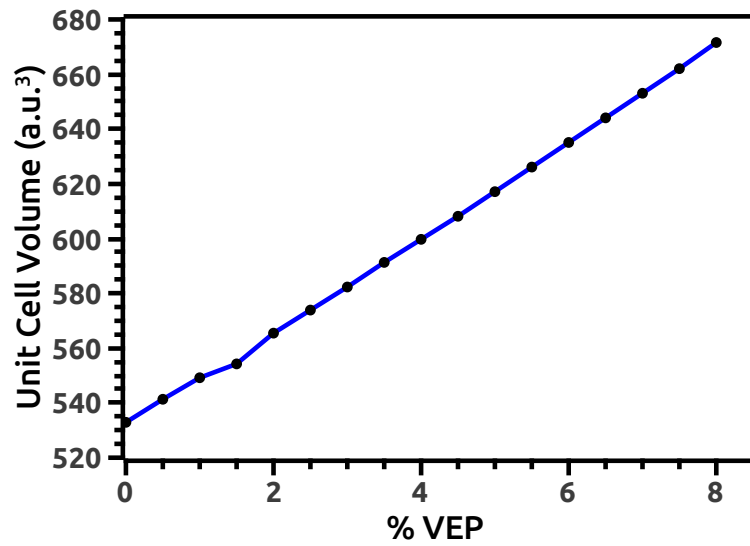


Figure 3: Increment in the unit cell volume (a.u.³) due to VEP

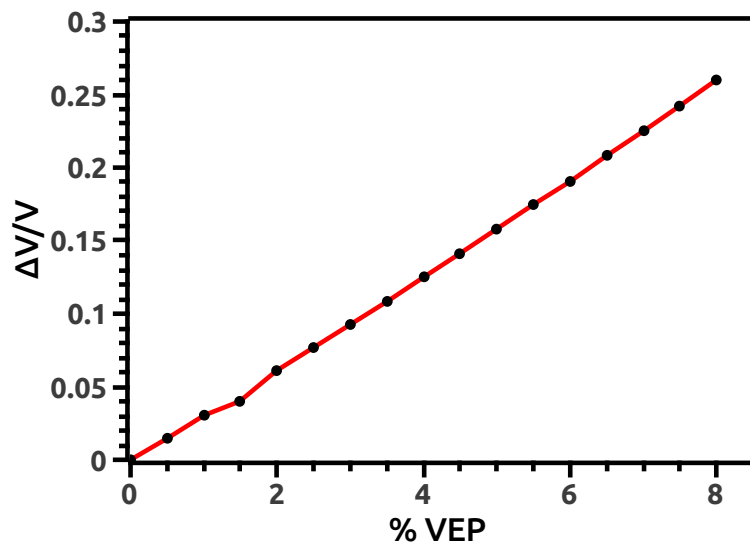


Figure 4: Volume strain with respect to % VEP

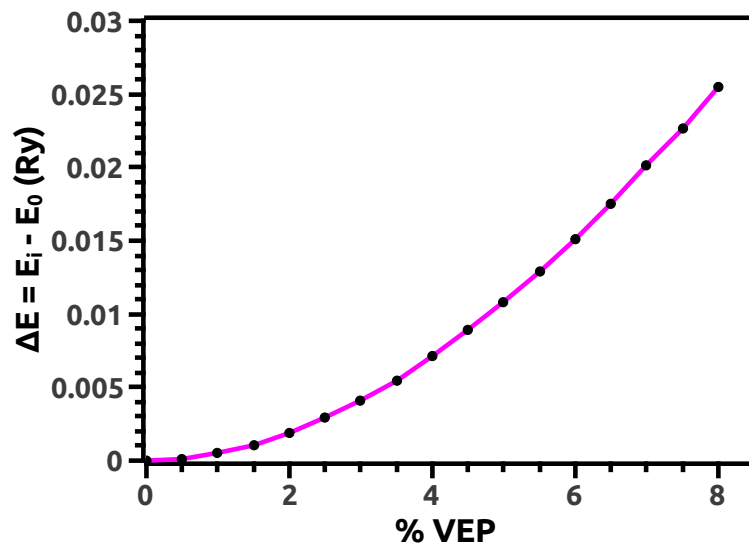


Figure 5: Change in Total Energy (Ry) of the system indicating a shift from the equilibrium state leading to a quantum phase transition.

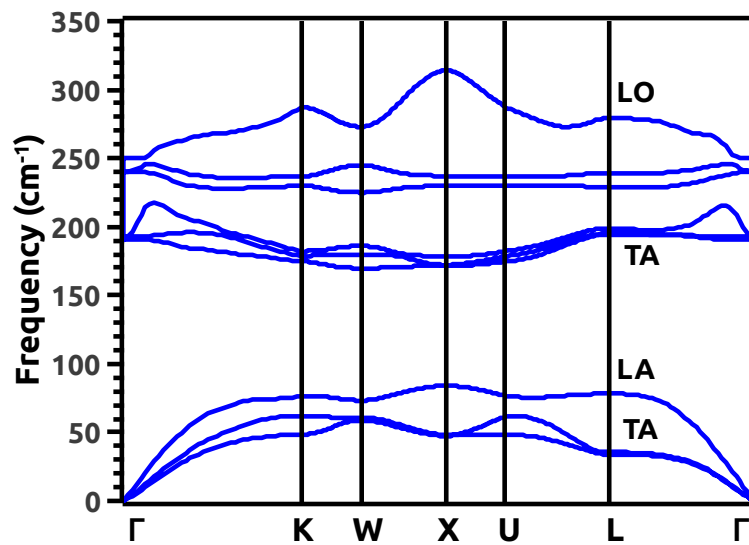


Figure 6: Phonon Dispersion Curves at 0% VEP

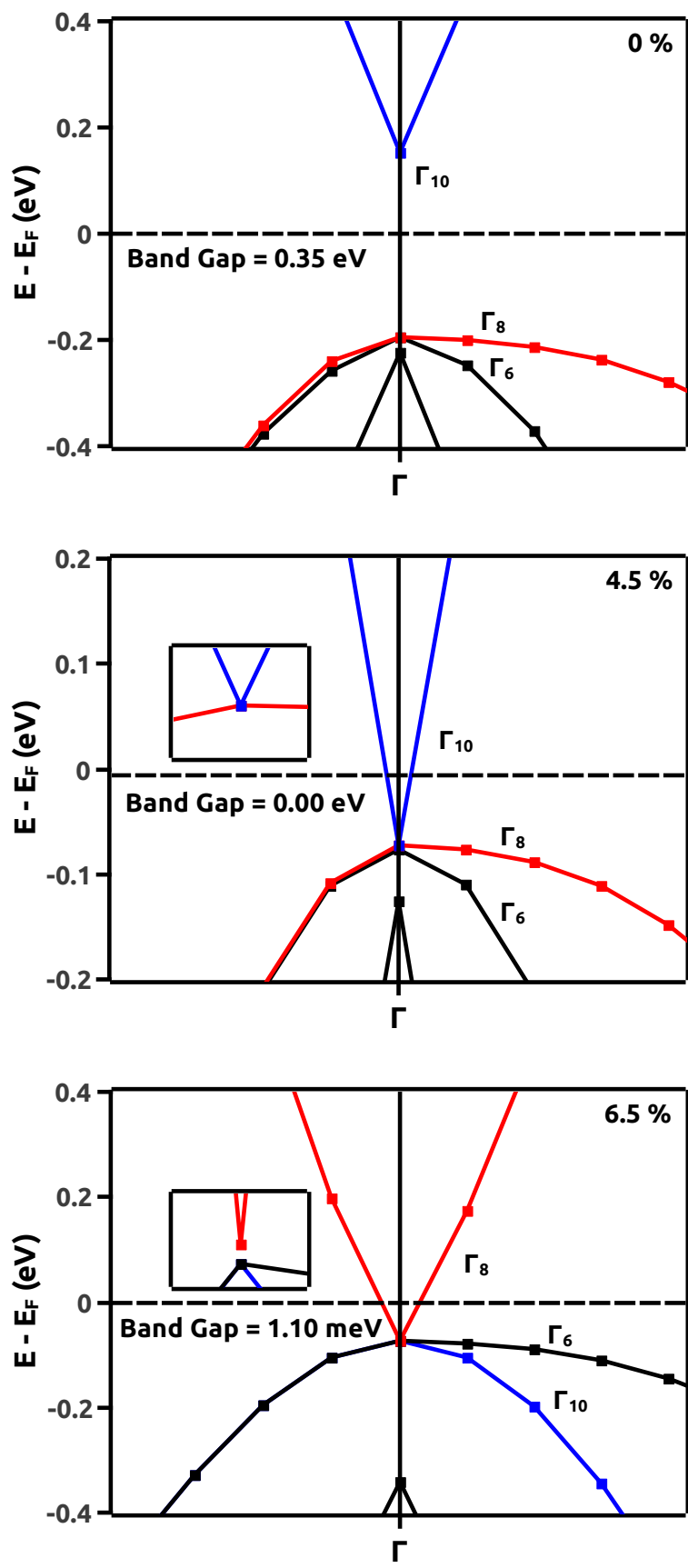


Figure 7: EBS at 0%, 4.5% and 6.5% VEP

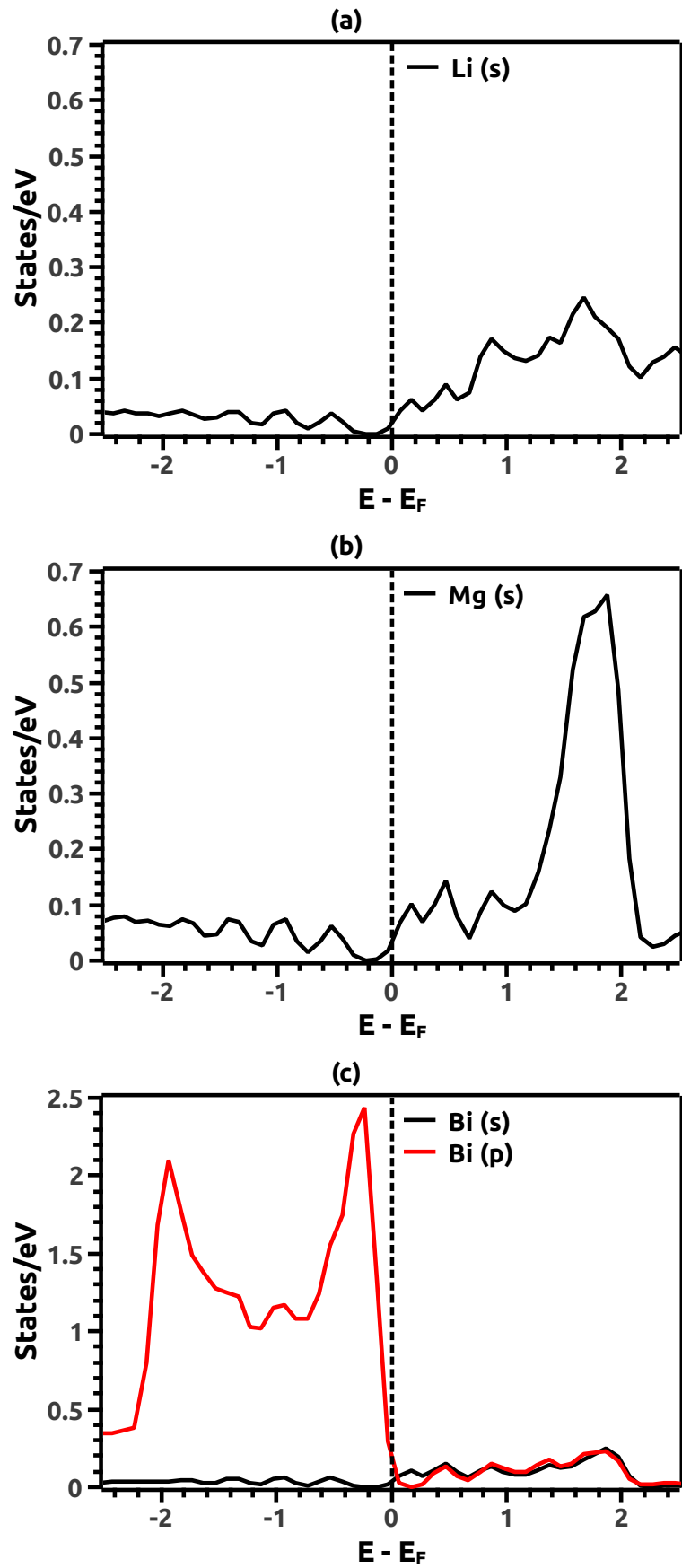


Figure 8: LDOS of (a) Li, (b) Mg and (c) Bi at 0% VEP

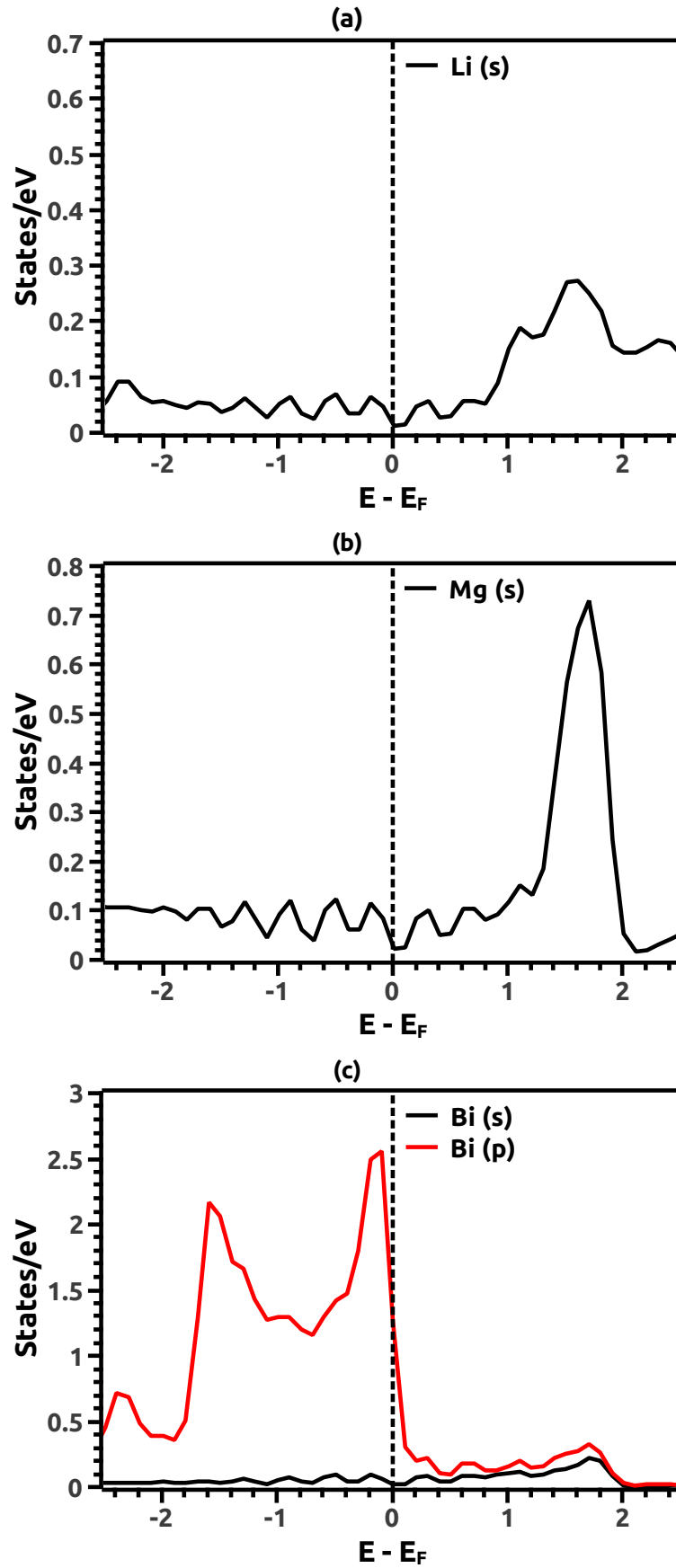


Figure 9: LDOS of (a) Li, (b) Mg and (c) Bi at 4.5% VEP beyond the critical value

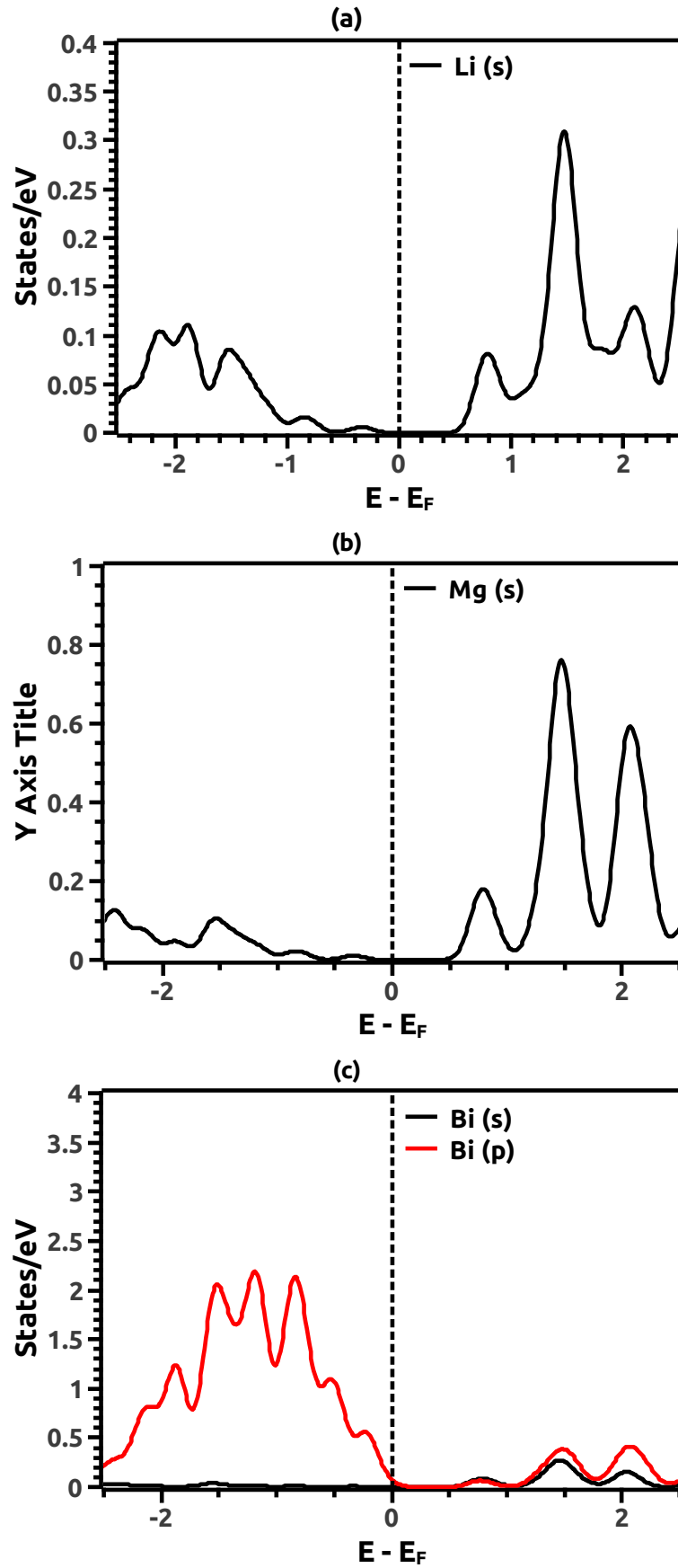


Figure 10: LDOS of (a) Li, (b) Mg and (c) Bi at 6.5% VEP indicating band inversion

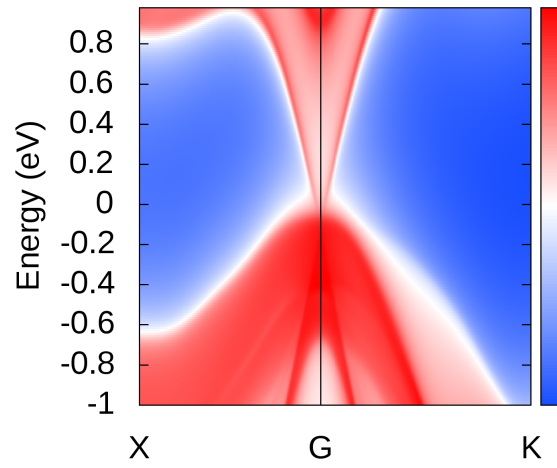
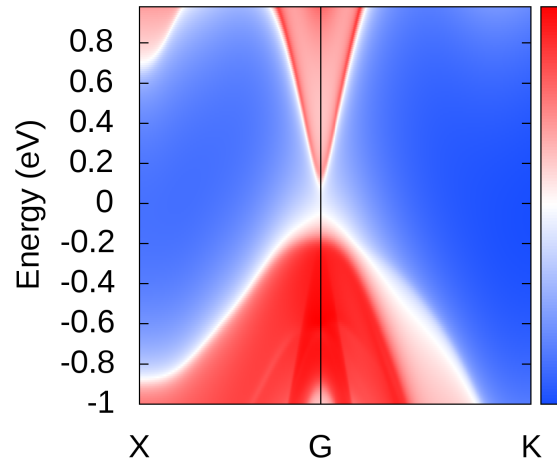


Figure 11: Surface States (computational ARPES) at 0% and 4.5% VEP obtained using WT

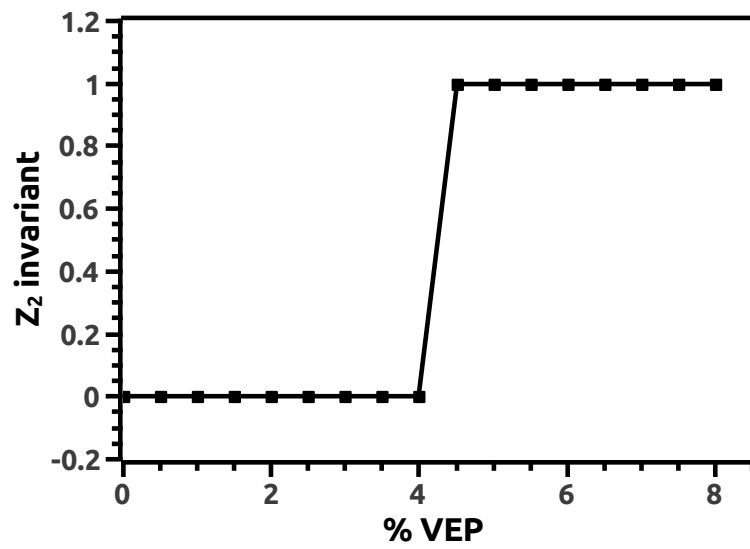


Figure 12: Z_2 evolution along the applied % VEP